Performance of Cement Mortar with Inorganic $Na_2SO_4 \cdot 10H_2O$-$Na_2HPO_4 \cdot 12H_2O$ Shape-Stabilization Phase Change Materials

Xiaonan Wang[1]; Wengui Li[2]; Yipu Guo[3]; Kejin Wang, F.ASCE[4]; and Yuhan Huang[5]

Abstract: Phase change material (PCM) is a strategic choice for storing energy and regulating the building temperature. It has been successfully integrated into cement-based materials, significantly affecting mechanical properties. The main feature of PCM is thermal mass control, given the sensitivity of the hydration process to temperature. In this study, multiple methods were applied to investigate the changes in cementitious mortar caused by the addition of PCM. Eutectic hydrated salt and expanded perlite (EP) were used to fabricate an inorganic shape-stabilized PCM composite known as EPC. The influence on hydration is directly reflected in internal temperature change, volume shrinkage, and mechanical properties. In addition, microcharacterization was used to reveal the underlying reasons. The EP-based mortar did not exhibit weaker mechanical properties but showed a higher volume shrinkage. The alkalinity of the PCM was not sufficient to trigger the activity of amorphous silica (SiO_2) in the EP, and this difference was attributed to its physical properties. The EPC demonstrated remarkable temperature regulation during hydration, replacing the temperature peak with a plateau. The residual sodium sulphate decahydrate ($Na_2SO_4 \cdot 10H_2O$) on the surface of the EP promoted ettringite generation near the aggregate, contributing to a slight volume expansion in the early stage and a decrease in the cement–aggregate bond quality. This phenomenon significantly accounts for the strength loss in the PCM mortar. The heat flow during hydration was altered, resulting in lower peak temperatures and a lower final hydration level. In conclusion, not only is PCM incorporation critical, but the choice of PCM type is also crucial for concrete properties. Therefore, the selection of the PCM should consider its potential effect on hydration, placing a higher demand on leakage prevention.

Author keywords: Phase change material (PCM); Cement hydration; Volume shrinkage; Temperature regulation; Energy-saving.

Introduction

PCM Concrete Benefit and Development

The energy crisis is a severe challenge from pole to pole. The traditional construction area requires enormous power and material, leading to large energy consumption. Phase change material (PCM) is an alternative solution to energy management that has been proven in various applications including battery (Cao et al. 2020), construction (Wang et al. 2022), renewable energy storage (Hosseinzadeh et al. 2021), and so on. Apart from energy saving, PCM can relatively maintain a stable temperature that is required for buildings to offer a comfortable living temperature (Islam and Ahmed 2021). The PCM application in construction is various including windows (Li et al. 2022; Ravasio et al. 2021), ventilation systems (Chen et al. 2023; Hu et al. 2021), and the main structure that is generally made of concrete (Adesina 2019; Kuznik et al. 2011; Zhang et al. 2020). Therefore, researchers have been working on modifying concrete with PCM for energy saving and room temperature regulation (Akeiber et al. 2016; Cui et al. 2022b; Zhang et al. 2020), when the multifunctional PCM concrete is also attractive to three-dimensional (3D) printing (Cui et al. 2022a), electromagnetic shielding (Xie et al. 2023), self-compacting technology (Hunger et al. 2009), and so on.

The incorporation of PCM in the main building structure is divided into three types: macro-encapsulation PCM (macro-PCM), micro-encapsulation PCM (micro-PCM), and shape-stabilization PCM (SSPCM) (Wang et al. 2022). The macro-PCM is normally used as a separate part such as a PCM layer or PCM tubes in a combined wall (Hou et al. 2023; Rathore and Shukla 2020). The micro-PCM and SSPCM are usually mixed with building materials and is a critical topic (Drissi et al. 2019; Wang et al. 2023). The primary requirements for PCM incorporation are thermal effectiveness and little adverse effect on matrix material such as concrete.

The advantages of PCMs on energy saving, temperature regulation, environmental protection, and so on, have been successfully highlighted. Yu et al. (2022) investigated the economic performance of cement mortar incorporated with novel SSPCM of 20 vol% (by sand). The annual energy saving was evaluated as 0.248 kW · h=kg

[1]Ph.D. Candidate, School of Civil and Environmental Engineering, Univ. of Technology Sydney, Sydney, NSW 2007, Australia. Email: xiaonan.wang@student.uts.edu.au

[2]Scientia Associate Professor and ARC Future Fellow, Centre for Infrastructure Engineering and Safety, School of Civil and Environmental Engineering, Univ. of New South Wales, Sydney, NSW 2052, Australia (corresponding author). ORCID: https://orcid.org/0000-0002-4651-1215. Email: wengui.li@unsw.edu.au

[3]Ph.D. Candidate, Centre for Infrastructure Engineering and Safety, School of Civil and Environmental Engineering, Univ. of New South Wales, Sydney, NSW 2052, Australia. Email: yipu.guo-1@student.uts.edu.au

[4]Professor, Dept. of Civil, Construction, and Environmental Engineering, Iowa State Univ., Ames, IA 50011. Email: kejinw@iastate.edu

[5]Senior Lecturer and ARC DECRA Fellow, School of Civil and Environmental Engineering, Univ. of Technology Sydney, Sydney, NSW 2007, Australia. Email: yuhan.huang@uts.edu.au

and a cost saving of 0.124 CNY=kg was expected. The CaO_2 emission reduction was estimated to be up to 0.27 kg=kg, which benefited the environment. To improve the efficiency, Zhang et al. (2022) simulated the dynamic PCM layer embedded in the wall. The static PCM layer could reduce the heating period by 13% while the dynamic PCM layer enhanced the saving to 89% in the cold winter. Elmarghany et al. (2022) filled the cylinder voids of the brick by PCM while the volume contributed 27% to the whole brick. The ambient condition was set based on the hot climate of Egypt. Among the PCMs in this experiment, n-Eicosane showed the best performance with the lowest maximum temperature and heat flux. The year-long simulation calculated the energy saving as 18.7% and the efficiency in winter was the highest. Arumugam and Shaik (2021) calculated the PCM-filled bricks under the local dry–hot conditions where the optimal air-conditioning cost saving reached to over USD 90 annually and the annual reduction of CO_2 approached 4 t. At the same time, the payback period was reasonable (8.5 years), considering that the lifetime of buildings was over 50 years. Mi et al. (2016) simulated the benefits of PCM with a melting point of 27°C in Chinese cities. Based on this design, the PCM showed better effectiveness in cold environments. When the effectiveness drops down, such as in Kunming and Hong Kong, the investment may not be deserved from an economic viewpoint.

In addition to the energy and environmental issues, specific PCM concrete can bring interesting benefits, such as low-temperature PCM concrete to melt snow and reduce freeze–thaw damage. Deicing salt has been popular for decades, but the damage can destroy concrete structures (Farnam et al. 2015). In this case, PCMs with a low transition temperature may release the heat to prevent ice and snow. The released heat was significant with organic PCM addition (Farnam et al. 2016), although further work should be completed to solve relevant problems, including weaker strength, lower elastic modulus, stability of PCM, and so on. Esmaeeli et al. (2018) incorporated PCMs with a low transition temperature with expanded shale to design slabs. In the temperature range of −10°C to þ10°C, a time lag of 9 h was found for temperature dropping to 0°C. A numerical model was proposed and verified by the laboratory experiment, which was used to simulate the performance in over 200 cities in the United States considering different climates. In most cities, the freezing time and depth were reduced by over 10%, proving the wide applicability, although the effectiveness was varied.

Deb et al. (2024a) tested micro-PCM and SSPCM with a similar transition temperature of 3°C–6°C at different temperature-changing rates. A decreasing rate over 1°C=min made an obvious supercooling interfering with the advantage of PCM, which was not a challenge for most outdoor environments. The pore effect (pore size of porous material in SSPCM, the particle size of micro-PCM) was proposed in that large pores ($r > 17.3$ nm) allowed free transition and energy release. In addition, they investigated the performance of snow melt (Deb et al. 2024b). Under light snow with depths of 1.8 and 4.3 cm (0.7 and 1.7 in.), a convincing result was completed. It was proposed that the ambient temperature should not kept at a low temperature before snowfall, which may eliminate the heat release of PCM. Although both SSPCM and micro-PCM had remarkable heat release performance in the laboratory, SSPCM was recommended in realistic applications because of the wider range of transitions.

Urgessa et al. (2019) designed a micro-PCM based on paraffin with a transition temperature of 4.5°C and cast a concrete slab. Based on the weather in November in Seongnam, South Korea, temperature drop was significantly delayed, leading to fewer freeze–thaw cycles and weaker incidental deterioration. Furthermore, the service life was expected to be extended by 20.7%–35.9%, contributed by a 20% PCM addition. They proposed that the temperature fluctuating around the transition point could improve the PCM effectiveness. The reduction of mechanical properties was found to be 22%–47%. Haider et al. (2022) also met the issue with a reduction of 29%–39%. The SSPCM with a melting point of 4.18°C was coated with conductive epoxy resin. To improve the strength, a second coating layer of silica fume was applied, and carbon nanotube (CNT) suspension was added to the sample casting. This method eliminated the strength loss by up to 20%, which was attributed to denser mortar and a stronger interfacial transition zone (ITZ).

Unexpected Changes and Reasons

The low strength is the most universal difficulty of PCM concrete. Fang et al. (2023) designed artificial geopolymer aggregates to absorb PCM, which had a good melting enthalpy of 4.29–24.74 J=g, a temperature stability up to 10.5°C, and a reduced lower carbon footprint, but the crushing strength of the PCM aggregate dropped by 4.13%–25.46%, although the authors believed that the residual strength was still desirable. Pilehvar et al. (2019) tested portland concrete and geopolymer concrete with micro-PCM particles (up to 20% replacement of sand) under freeze–thaw cycles. Before cycles, the lower compressive strength of the concrete was obvious due to the addition of weak micro-PCM. The compressive strength reduction after cycles was common but the addition of micro-PCM in concrete decreased the strength by 2.5% or lower, which proved the improved resistance against freeze–thaw cycles. Pilehvar et al. (2017) observed the weak connections and air voids around micro-PCM particles that caused weak bonds. The compressive strength reduction showed a linear relationship with the PCM content. Li et al. (2019) designed an SSPCM based on lightweight aggregates smaller than 5 mm while the core PCMs had melting points of 1°C–3°C, 3°C–5°C, and 5.2°C. In this work, the SSPCM replacement of 50% in the concrete sample was enough to provide an excellent delay in pore water freezing. It was recommended that the solidification of PCM started prior to water, which enabled the exothermic energy to delay water freezing. Brooks et al. (2021) used fly ash cenosphere as the supporting material for SSPCM. The rigid shell (compared to commercial polymer-coating PCM) and pozzolanic activity of the cenosphere improved the strength of the PCM mortar. Snehal et al. (2020) proposed the incompatibility of PCM with a cement system that caused higher permeable porosity. Furthermore, it was vulnerable to various aggressive conditions where significant loss in density, strength, and volumetric stability were found (Snehal et al. 2022). Much endeavor is required to investigate the reason for weak PCM concrete and to propose an effective solution.

The mechanical adjustment could be various. Cui et al. (2022b) designed a hollow steel ball with a diameter of 19 mm to encapsulate the PCM and added in concrete for the energy pile. A large reduction in compressive strength was initially observed, but the increase in ball thickness could mitigate this reduction. As a result, 0.7% steel fiber was recommended to improve both strength and conductivity. Another significant revelation was the higher ductility caused by both steel ball and fiber. The worse volume stability was also a critical impact. Snehal et al. (2020, 2022) proved the obvious compressive strength reduction of mortar with different PCM types. The reduction percentage varied with PCM types and dosages, while the nanosilica was incorporated to compensate for this problem. Xu and Li (2014) fabricated a paraffin–diatomite aggregate for engineered cementitious composite (ECC). Apart from the improved thermal storage, this aggregate brought larger shrinkage deformation.

Ramakrishnan et al. (2017) observed a similar trend for paraffin–expanded perlite mortar and attributed it to the lower stiffness of the PCM composite. The higher PCM composite content caused a higher shrinkage of mortar. Snehal et al. (2020) observed the advantageous effect of *n*-octadecane–based PCM on chemical shrinkage. They proposed that the heat storage of PCM minimized the thermal variation that reduced the chemical shrinkage. Ren et al. (2021) tested the increasing autogenous shrinkage after microencapsulated-PCM addition, which was explained by additional pores and an uneven distribution of free water. Kumar et al. (2022) found increasing compressive strength and thermal conductivity with PCM loading when the PCM had an absorption lower than 75%. No leakage was observed. They attributed these to a lower water–cement (w=c) ratio and a higher particle density.

Concrete is a temperature-sensitive material, especially at an early age. Crack generation is universally fatal for concrete while the critical factor, temperature, could be affected by the PCM (Šavija and Schlangen 2016; Xue et al. 2019). From one side, the temperature distribution makes the stress difference. This theory is also applied to freeze–thaw damage of concrete (Šavija and Schlangen 2016) and reduces the stiffness loss (Nayak et al. 2019). On the other side, the cement hydration process is significantly influenced by temperature changes (Šavija 2018). Snoeck et al. (2016) concluded that the PCM could reduce stress and strain leading to less thermal cracking, which was made by the delayed temperature rise. In other words, the deformation of concrete could be influenced by the PCM. Snehal et al. (2020) presented the cement hydration interruption caused by PCM addition. The *n*-octadecane PCM raised the Ca–Si ratio, and a nanosilica addition of 3% effectively repaired the issue. Currently, most experiments analyzed the mechanical properties of PCM concrete from the perspective of physical factors. The influence of PCM on cement hydration has rarely been presented in papers.

Objectives and Significance of This Work

The advantages of PCM on concrete have been proven, and the current aspiration is to focus on improving the benefit efficiency and eliminating the adverse effects. From the literature, the various drawbacks on mechanical properties and durability are observed, and there has not been a comprehensive explanation. PCM addition may affect the cement hydration that generates a vital influence on concrete. From this perspective, this work investigates the shrinkage performance and strength changes of PCM mortars.

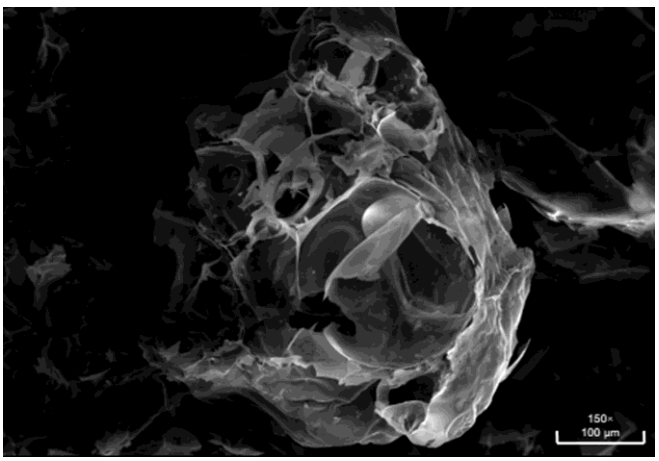

Fig. 1. Morphology of raw EP.

The temperature evolution in the hydration process and isothermal calorimetry are tested to directly reveal the influence. Then, effective characteristic methods and microstructures illustrate the results of this influence, and further explain the change of strength and durability.

The PCMs' impact on cement hydration has not been fully understood considering various PCM types and concrete design methods. This paper offers valuable analyses to uncover a relationship between PCM composite and cement-based systems. The selected PCM and incorporation method are commonly used and have a wide application range. The theory of how PCM (inorganic hydrated salt) makes an effect is proposed, and accurate changes for physical performance are evaluated. This enriches the data for the inadequate research about PCM concrete, especially from the viewpoint of cement hydration. The tested result is analyzed with crucial parameters for realistic applications, which helps the development of PCM concrete design with stable strength and durability, including the selection of raw materials and effective modification.

Experimental Program

Raw Materials

The disodium hydrogen phosphate dodecahydrate [$Na_2HPO_4 \cdot 12H_2O$ (NHP)] and sodium sulphate decahydrate [$Na_2SO_4 \cdot 10H_2O$ (NS)] were purchased in Australia and selected as core PCMs in this work and they both showed effective results in building material for energy saving (Hirschey et al. 2022; Islam and Ahmed 2021; Rao et al. 2018). NHP was provided by Glentham Life Sciences and NS was manufactured by Thermo Scientific, which had a purity of 99%.

The expanded perlite (EP) is a common lightweight aggregate for mortar and concrete, and it is good at absorbing PCM due to its high porosity (Ramakrishnan et al. 2015; Sun et al. 2023; Zhang et al. 2016) as shown in Fig. 1. The EP was purchased from Ausperl Australia with a dry density of 70 kg=m^3 and a volume porosity of 65%. The size distribution is provided in Table 1 (AUSPERL 2021). The EP was stored in a room with low humidity and was dried in an oven at 80°C, lasting for 24 h before the experiment every time.

The silica sand (SS) with a small size (~1 mm) and general-purpose cement was used in this experiment, which was stored in a room with low humidity. Bastion general-purpose cement, produced in Australia, consisted of portland cement (>92%), a little limestone, and gypsum according to the technical sheet from the company. The polycarboxylate-based superplasticizer [(SP) Sika VescoCrete-140 KS] was used to modify the flowability.

PCM Composite Preparation

This experiment designed a eutectic PCM by mixing NHP and NS with a weight ratio of 1∶1 (at solid state). The NHP and NS were sealed in vessels and mixed by ultrasonic in a water tank at 40°C. In this procedure, the NHP and NS became liquid state. The EP was heated at 50°C and 80 kPa in a vacuum oven for 12 h to remove the

Table 1. Size grade of EP

Size (mm)	Percentage (%)
0.15–0.3	5–30
0.3–0.6	10–40
0.6–1.18	30–60
>1.18	0–40

Source: Data from AUSPERL (2021).

pore moisture and air (it was previously kept at 80°C, as aforementioned). According to the capability information from the manufacturer, the water holding capacity by volume of the EP was 65%. The incorporation mass ratio of 10:6 (PCM: EP) was selected, which equaled 7:60 by volume. This ratio is much lower than the water holding capacity that is supposed to achieve thorough impregnation and be leakage free.

The EP–PCM composite is abbreviated as expanded perlite–PCM composite (EPC). The weighted EP and PCM (liquid) were mixed in the container before vacuum pumping. The vacuum oven was set at 40°C and 50°C and 80 kPa for 4 h to allow the liquid PCM filling the pores of EP. Finally, the heater was turned off and the vacuum pump kept working to enable the temperature of PCM composites to reduce to room temperature and obtain the solid PCM composites.

Mortar Mixing Design

This experiment separately designed three groups of mortar with different aggregates (SS, EP, and EPC): silica sand–based mortar (SSM), expanded perlite–based mortar (EPM), and expanded perlite–PCM composite-based mortar (EPCM). The cement–sand weight ratio of the basic group (SSM) was 4:9, while the aggregate replacement ratio was 100% based on volume for the other groups (EPM and EPCM). The mass difference of aggregates was large because of the extreme low density of EP. The mixing proportion is provided in Table 2. The extra water and SP in EPM and EPCM modified the flowability because much water was absorbed by the EP. Three groups had the flowability range of 180–200 mm. All samples in this paper had the same dimension of 40 × 40 × 160 mm. For the shrinkage test, the length (160 mm) included the length of the gauge studs. In other words, the designed distance of the ends of the gauge studs was 160 mm (BSI 2002) and the length of the mortar prism was 150 mm (AS 2006).

Methodology

Hydration Performance Using Isothermal Calorimetry

The isothermal calorimetry test was performed using I-Cal 4000 (manufactured by Calmetrix USA) with four channels. According to the user guide, two reference metal cylinders were used for each channel. The quantified testing sample was sealed in a plastic container that fitted well with the sample channel. The details of sample mixing for each channel are provided in Table 3. The container filled with tap water was placed in channel 1 as a reference and calibration. The SSM, EPM, and EPCM were tested in channels 2, 3, and 4, respectively. The mixing plan of each group had the same proportion as that in Table 2. All channels were turned on 24 h in advance to maintain the stable thermal environment of the channels. The channel temperature was set as 25°C, which was required by standards for mortar curing. Before the test, the cement and aggregate were weighed and mixed thoroughly in the container for each group. Similarly, the water and SP were weighed and mixed. Then, the water with the SP was added to the container, followed by fast manual mixing for 20 s. The time of water addition was recorded as the start of hydration. All containers with designed samples were placed in the channel quickly. The heat flow in the first 4 days was collected and analyzed.

Table 2. Details of mortar mixing proportion

Mortar	Cement (g)	Water (g)	SS (g)	EP (g)	EPC (g)	SP (g)	w=c	SP=c (%)
SSM	488	195.2	1,098	—	—	3.66	0.4	0.75
EPM	488	219.6	—	50	—	4.88	0.45	1
EPCM	488	219.6	—	—	133.3	4.88	0.45	1

Table 3. Tested mortar sample in each channel of isothermal calorimetry

Channel	Cement (g)	Aggregate type	Aggregate mass (g)	Water (g)	SP (g)
1	—	—	—	30	—
2	20	SS	45	8	0.15
3	20	EP	2.05	9	0.2
4	20	EPC	5.46	9	0.2

Temperature Change during Hydration

The temperature was collected using K-type thermocouples connected to a data logger. The thermocouples were embedded in the sample during casting. The temperature collection started when the mortar cast was completed. The time gap between water addition in mixing and the first temperature collection was recorded. The time interval of each collection was 10 min. On the first day, the samples were cured at a room temperature of ~24°C with plastic film coverage. Over the next days, the samples were cured in a water tank with a temperature of ~22°C, as shown in Fig. 2.

Characteristics of Hydrated Products

Many reliable test methods were applied to analyze the features of hardened mortar, including X-ray diffraction (XRD), Fourier-transform infrared spectroscopy (FTIR), and scanning electron microscopy–energy-dispersive spectroscopy (SEM-EDS), which are popular in building material characteristics. The SEM was also able to provide microstructure performance. The sample for XRD and FTIR was milled into fine powder. The XRD test was completed using Bruker D8 Discover XRD to identify the mineralogical characterization with a 2θ scan range from 5° to 70°.The total number of steps was 3,526 with 0.8 s per step. The whole scan for each test took 50 min. The FTIR test was completed using a Perkin Elmer Frontier IR spectrophotometer. The absorption spectrum was measured from 4,000 cm^{-1} to 400 cm^{-1} with a resolution of 2 cm^{-1}. Thermal gravimetric analysis (TGA) was set from 25°C to 1,000°C with the heating rate of 10°C=min. The SEM-EDS test was completed using Zeiss EVO LS15 at the low magnification of 500× and Zeiss Supra 55VP at the high magnification of 10,000×.

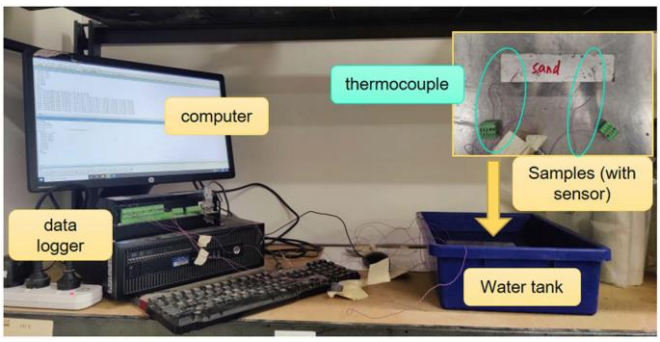

Fig. 2. Configuration for temperature collection.

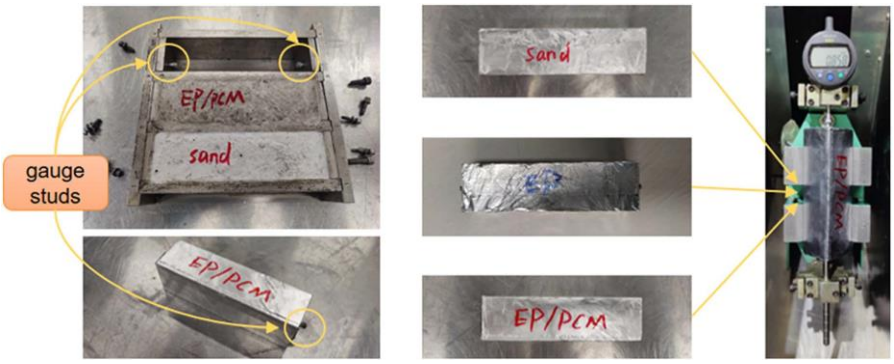

Fig. 3. Samples and apparatus for the shrinkage test.

Shrinkage and Strength

The shrinkage test and calculation followed standard C157/C157M-17 (ASTM 2017). The cast samples were covered by plastic film and cured at room temperature on the first day. After 24 h, the samples were demolded and tightly covered by the aluminum film as shown in Fig. 3. The distance between the end of the two gauge studs was recorded as a reference. The shrinkage performance in the following days was calculated based on this reference length. The moisture evaporation was an important reason for the shrinkage so that the aluminum coverage eliminated the influence of evaporation (Song et al. 2016). The obtained shrinkage was mainly caused by hydration reaction and temperature change. All samples were placed on the shelf in the shrinkage room, where the temperature was 22.5°C and the relative humidity was 48%.

The 3-point flexural strength and compressive strength were tested on the hydraulic compression machine with the required apparatus. The compressive strength of mortar was tested after 28-day standard curing based on the specimens' portion of prisms made and broken in the flexural strength test. According to standards C349-18 and C348-21 (ASTM 2018, 2021), the loading speeds were set as 44 N=s and 1.3 kN=s for flexural and compressive strength tests, separately. After being cured at room temperature with plastic film coverage for 24 h, the samples were demolded and cured in the water tank until the day of testing.

Results and Discussion

Temperature Evolution

The test lasted for over 4 days as shown in Fig. 4. From Fig. 4(a), all samples showed temperature reduction and recovery before 10 h, which was marked as S1 caused by cement dissolution. Then, the huge amount of heat accumulation led to an increasing temperature, which was marked as S2. The EPCM showed a delayed increase that was caused by the thermal inertia of the PCM (Snoeck et al. 2016). The rapid hydration made the temperature peak for the SSM and EPM. After that, the downward temperature suggested the lower hydration ratio. The peak intensity was different because it was affected by various factors including the w=c ratio, SP dosage, and so on. The SSM showed later acceleration and a lower speed. The trend was same although the expression level was changing. The critical difference was the temperature plateau (~27.8°C) for the EPCM sample, which was caused by the heat absorption of PCM. This plateau occurred at both S2 and S3, which were significant for cement hydration. The distinct plateau of the EPCM, especially compared to the EPM, regulated the ambient condition, leading to an unexpected hydration process. The S4 was normally regarded as a stable period. The difference was still observed but the gap was narrowed with time, while the temperature of the EPCM was higher than the EPM counterpart. Two reasons were

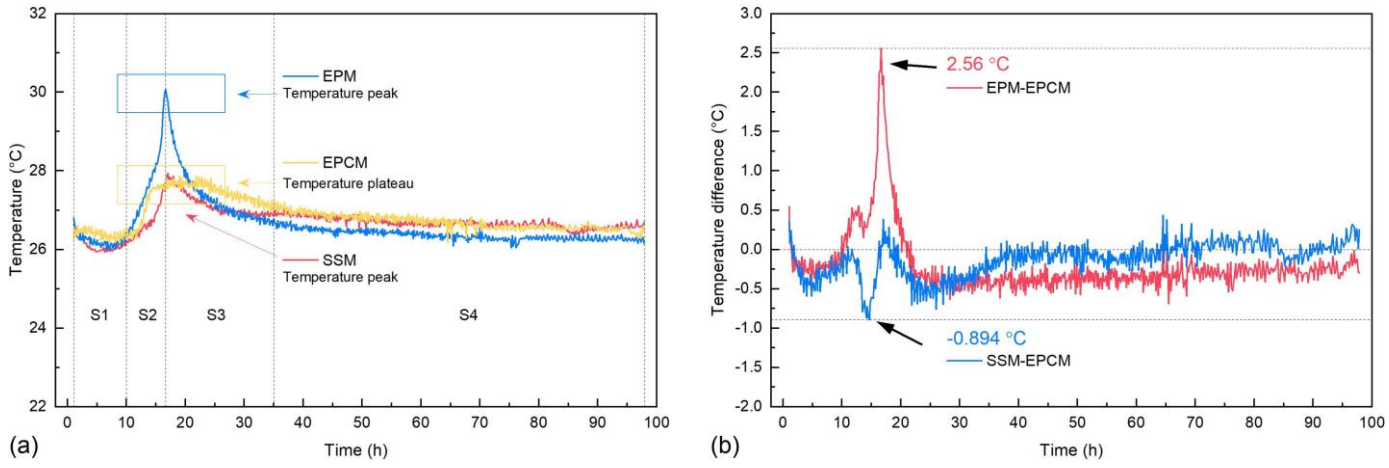

Fig. 4. Temperature evolution during hydration: (a) inner temperature of samples; and (b) temperature difference among samples.

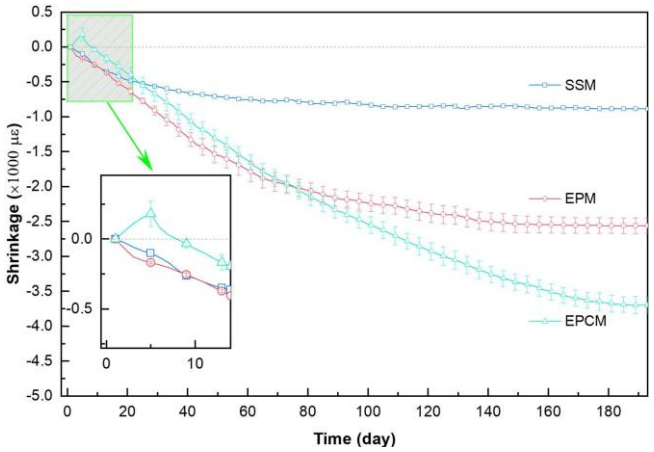

Fig. 5. Shrinkage results of mortar with different aggregate.

proposed. The first was the released heat from the PCM, which was the main feature of the PCM. The second was the delayed exothermic reaction in S2 and S3, which was continued in S4. Both reasons can also explain the bridged gap with the passage of time: exhausted energy storage and consumption of raw material. The gap was exhibited in Fig. 4(b), where the maximum value was 2.56°C and verged to 0°C over time. The effect concentrated from 12 to 20 h and still played a role until 97 h. It is noticeable that the curve is similar to the heat flow curve in the isothermal calorimeter, but the feature is different. The temperature is controlled by the specimen dimension, laboratory temperature, and curing condition, apart from the hydration performance. For example, the heat exchange with the curing water tank occurred in the temperature collection but the ambient condition in the isothermal calorimeter is stable. In addition, the temperature is a parameter of heat accumulation in the whole specimen that is less sensitive than heat flow. Thus, the temperature collection in the laboratory is complementary to heat flow data from the standard machine.

Shrinkage

As shown in Fig. 5, the SSM presented little shrinkage ability up to −875 $\mu\varepsilon$ and became stable from the 70th day, which was mainly contributed by the high stability of sand and less influence on cement hydration. The high water absorption of expanded perlite caused large deformation and the non-crystal quartz may lead to further reaction, in addition to the low strength of EP providing lower resistance against the shrinkage. All EPM and EPCM samples illustrated continuous shrinkage while the EPM became relatively stable from the 100th day and the EPCM accumulated the shrinkage steadily until the 178th day.

The critical feature of the EPCM was observed before the 8th day. The expansion occurred only on the EPCM that should be affected by the PCM while reaching 180 $\mu\varepsilon$ on the 5th day. The direct difference was the temperature plateau, as shown in Fig. 4, that could change the thermal expansion. The present paper showed the effect of PCM on expansion control (Šavija 2018; Šavija and Schlangen 2016). However, the lower temperature was supposed to reduce the expansion and the key corresponding time was unmatched: 15–25 h in temperature and 0–8 days in shrinkage. The sample dimension in this experiment was small, which mitigated the thermal effectiveness. Therefore, the reduced expansion by the lower temperature was limited and the varying product could be the main factor. The product could be influenced by two factors: temperature and the reaction with the PCM. The temperature regulated the reaction ratio and modified the hydration product, which may last for over 4 days (the peak of expansion occurred on the 5th day). The EPC was manufactured by vacuum impregnation without post process. The low quantity of the PCM posed little burden on leakage but the residual PCM on the surface during impregnation still may participate in a reaction. The expansion could be contributed by the NS, while the sulfate ion (SO_4^{2-}) was critical to the ettringite and gypsum generation that caused the expansion. Normally, sodium sulfate (Na_2SO_4) can accelerate cement hydration and increase the generation of calcium sulfoaluminate (or ettringite) showing an obvious expansion effect. The available Na_2SO_4 was limited, and the expansion was offset by the hydration shrinkage on the 8th day. The details required evidence from many following testing methods.

Mechanical Strength

As shown in Fig. 6, the EPM showed an increase on the compressive strength (16%) and flexural strength (9%) compared to the SSM. The strength of the EP was much lower than the SS, excepting the possibility of stronger aggregate supporting. The higher value could be caused by the cement matrix and bond. The EP had high water absorption that caused a stronger bond with the cement matrix and the matrix could be denser according to the large deformation in the shrinkage test, even though more water was used, which led to the higher strength. In addition, the non-crystal quartz of the EP may play a role in cement hydration, which can change the quality of the

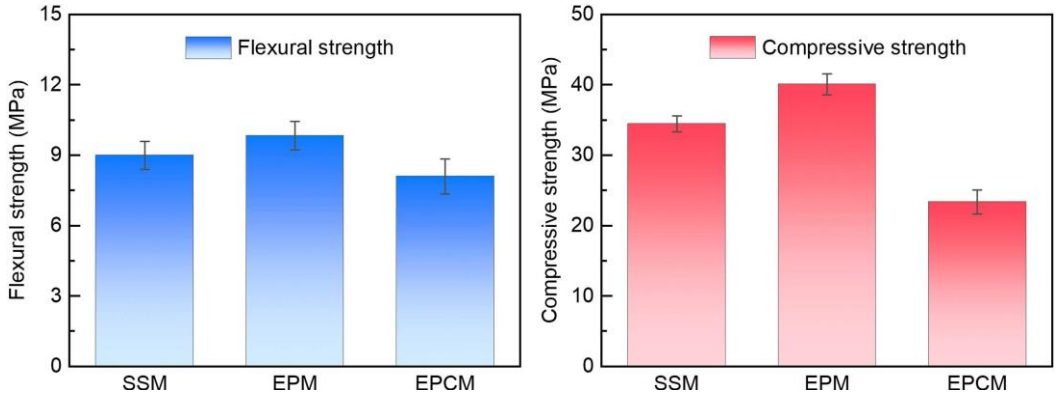

Fig. 6. Mechanical properties of specimens at 28 days.

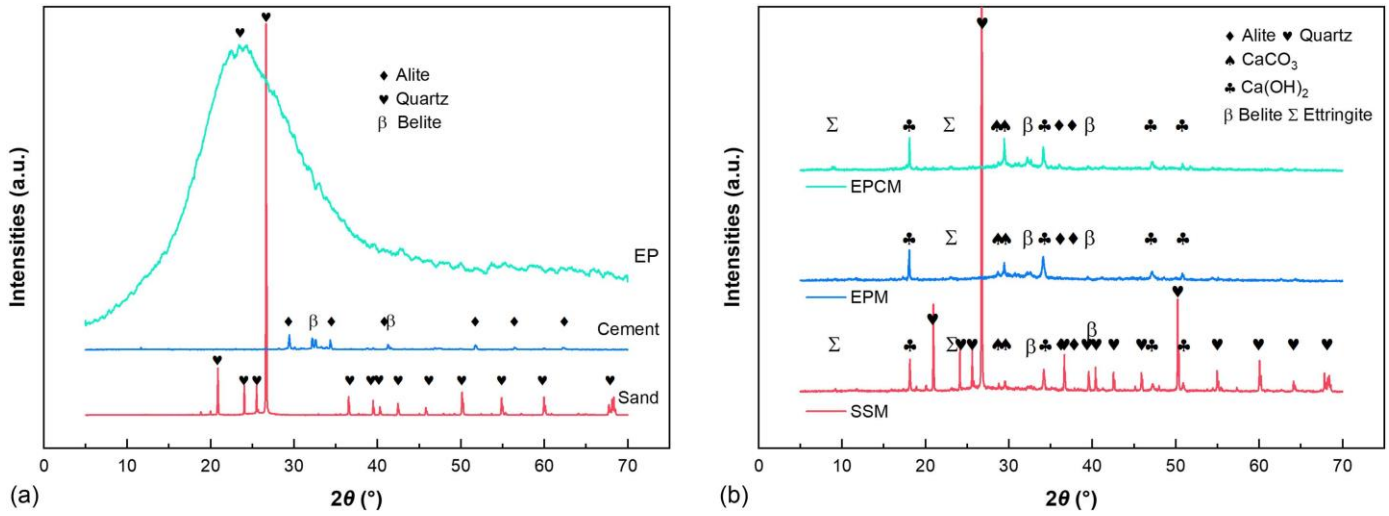

Fig. 7. XRD results for raw materials and hardened mortar: (a) raw materials; and (b) hardened mortar.

ITZ, and the analysis is provided in the next section based on characteristics. The rising compressive strength was limited by the weak EP when the aggregate strength was critical for the compressive strength. As previously explained, the porous EP improved the bond strength that benefited the bending resistance. The crack mostly occurred at the ITZ between the aggregate and the cement matrix. The reduction of the compressive strength on EPCM was evident (42%) while the flexural counterpart was mild (18%). The disadvantage could be explained by the lower capillary effect because the EP was partially filled by the PCM in advance. The enhancement on bond strength was eliminated and the crucial weakness of the EP became apparent. Similar to the explanation for shrinkage, the potential reaction caused by the PCM deserves much attention, because it can change the product around the aggregate and the property of the ITZ. In other words, the bond strength may suffer damage and the mortar become weak with the weak aggregate.

Characteristics (XRD, FTIR, TGA)

The XRD tests were performed for raw materials and hardened mortar as shown in Fig. 7. The peaks of the quartz in the SS were very strong, which indicated the stable crystal. Conversely, the quartz in the EP showed an amorphous state, which may participate in the hydration reaction or pozzolanic reaction. Most peaks of hardened mortar referred to universal mortar composition, including ettringite, alite, belite, calcium carbonate (Ca_2CO_3), and calcium hydroxide [CaðOHÞ$_2$]. The highest peaks of the SSM, which referred to the quartz, were contributed by the SS. The strong peaks at around 9° and 23° for the EPCM were ettringite. The NS attached on the surface of the EP closely contacted with cement particles and was likely to participate in the hydration reaction, which normally resulted in more ettringite generation. In other words, the phosphate was generally regarded as a retarder that would not change the final product. This conclusion was also applied to the NHP in this experiment and there was no crystal peak of hydrogen phosphate ðHPO$_4^{2-}$Þ-related product.

The pure and mixed PCMs were tested using FTIR in the range of 450–4,000 cm^{-1} to analyze the eutectic PCM manufacturing process as shown in Fig. 8. Because of water molecules, the obvious vibration of O─H was found at ~3,321 cm^{-1} and ~1,169 cm^{-1} for all samples. A significant vibration occurred at 1,300–500 cm^{-1}. The vibration as ~1,078 cm^{-1} and ~613 cm^{-1} referred to S═O and S─O, which was contributed by SO_4^{2-}. The vibration at ~1,187, 1,057, 979, and 854 cm^{-1} presented the existence of HPO_4^{2-}. All these key vibrations were observed for the NS–NHP and there was no new vibration. Although the mild vibration shift was detected, the stability of NS and NHP was still credible. There was not a new product, and the compatibility was reliable when the vibration shift was caused by the intermolecular attraction.

From Fig. 9, chemical bonds of cement hydration were found at ~1,411 and ~960 cm^{-1} referring to C─O and Si─O, which were key features of $CaCO_2$ and C─S─H. The O─H vibration was observed at ~3,637, 3,395 (wide), and ~1,640 cm^{-1}, which were contributed by a water molecule and CaðOHÞ$_2$. These vibrations were detected in all samples but the signal for SSM was relatively weak, especially for the O─H vibration. The amorphous quartz of the EP, with a very fine particle size as presented in Table 1, offered important raw material for the reaction, which boosted the hydration production. The increasing quantity and stability of products

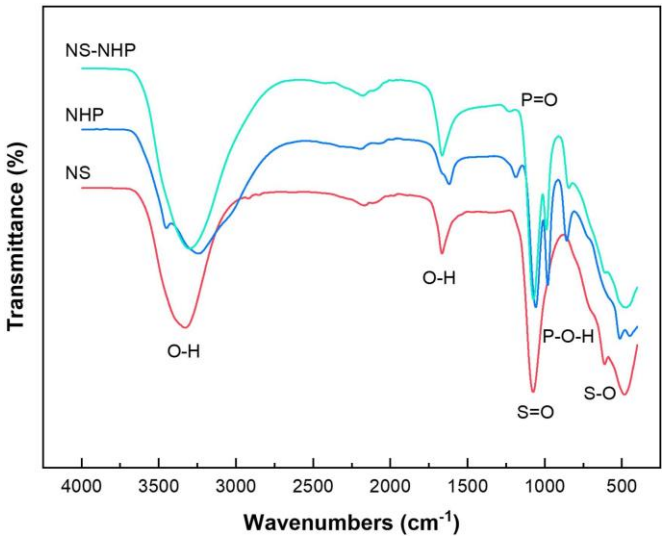

Fig. 8. FTIR results for PCMs.

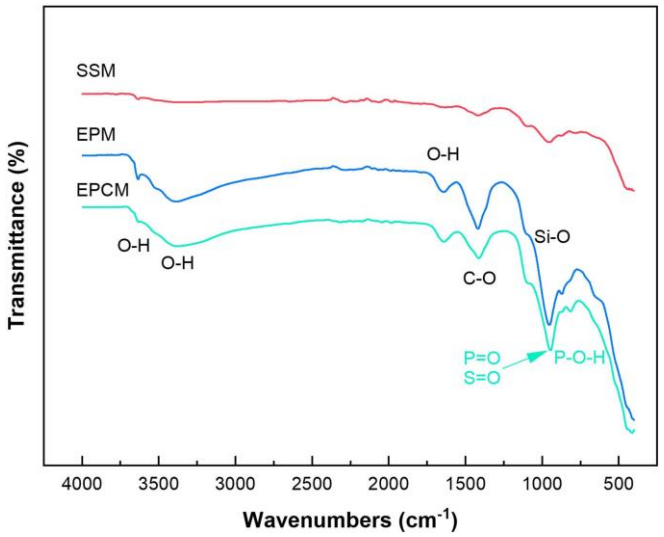

Fig. 9. FTIR results for hardened mortar.

contributed to the stronger vibration signals. For EPCM, the vibrations of PCM at ~1,000 cm^{-1} were covered by the Si─O, which was the most significant chemical bond in the hydration products. One vibration of P─O─H at ~845 cm^{-1} in the NS–NHP was still identified with a minor shift to ~816 cm^{-1}. The PCM incorporation showed little effect on the product composition but the amorphous quartz of the EP may effectively enhance the cement hydration.

The first mass loss was mainly caused by PCM dehydration, as shown in Fig. 10. The dehydration processes are presented in Eqs. (1)–(4). The dehydration of NS was direct and only one peak was found at 100°C as shown in Eq. (1). Three peaks were observed for NHP. The first two peaks referred to water molecule loss at 39°C and ~100°C as shown in Eq. (3), while the third peak at ~329°C showing the decomposition to tetrasodium pyrophosphate and water loss as shown in Eq. (4). These peaks were observed in NS–NHP, showing the compatibility in accordance with the FTIR result

$$Na_2SO_4 \cdot 10H_2O \rightarrow Na_2SO_4 + 10H_2O \quad (1)$$

$$Na_2HPO_4 \cdot 12H_2O \rightarrow Na_2HPO_4 \cdot 7H_2O + 5H_2O \quad (2)$$

$$Na_2HPO_4 \cdot 7H_2O \rightarrow Na_2HPO_4 + 7H_2O \quad (3)$$

$$2Na_2HPO_4 \rightarrow Na_4P_2O_7 + H_2O \quad (4)$$

For the water loss at 39°C, the material was sealed in the mortar so that the water molecule was not leaked. In addition, the dehydration was reversible when the temperature decreased. In most buildings working conditions, the temperature will not reach 100°C, where water changes to gas. Based on the TGA result, the NS–NHP was regarded reliable to work as a PCM in buildings. In extreme conditions such as a fire disaster, the dehydration and evaporation of this PCM could relieve the destruction. The deserved precaution was that this PCM mortar was not suitable as the stress-bearing part, which may be destroyed due to inner water evaporation.

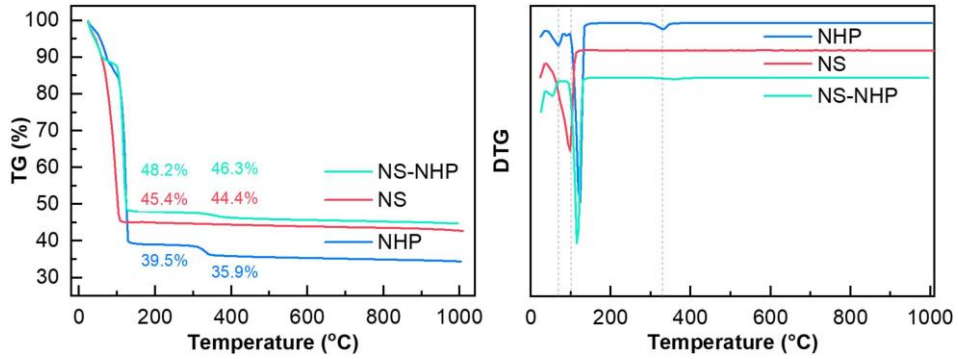

Fig. 10. TG and DTG results for PCMs.

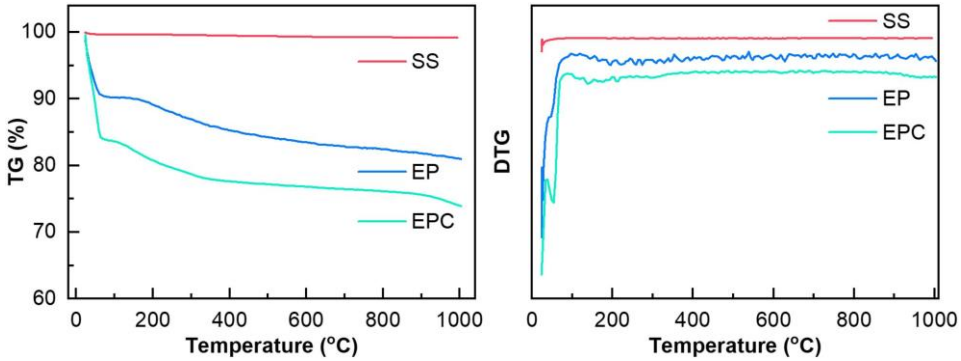

Fig. 11. TG and DTG results for aggregates.

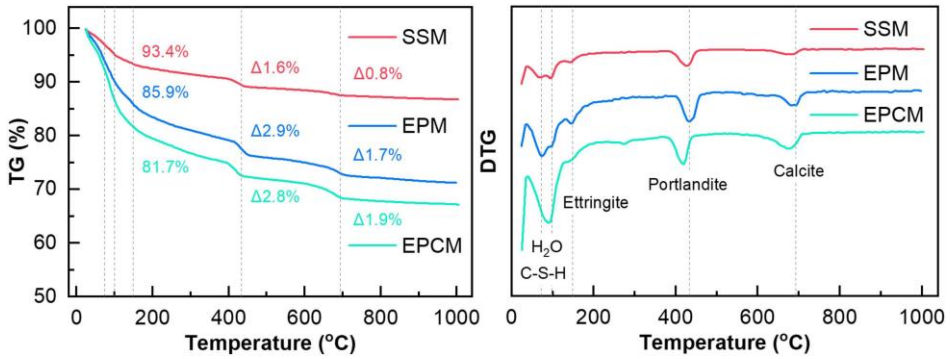

Fig. 12. TG and DTG results for hardened mortar.

As shown in Fig. 11, the SS showed extreme thermal stability while others had obvious mass loss up to 1,000°C. The loss of the EP was caused by impurities that were introduced during the expansion process in the factory. The further loss of the EPC mainly occurred at lower than 100°C and a peak was found in the derivative thermogravimetric (DTG) result, which was attributed to the dehydration of PCM. After 100°C, all samples showed reliable stability. The fluctuation in the DTG test was caused by the low total mass of the samples. The volume of the pan was limited and the low density made a low sample mass (~4 mg for EP, ~10 mg for EPC, and ~35 mg for SS). Therefore, the fluctuation of the EP was the most significant followed by the EPC counterpart.

After 28 days of curing, the hardened mortar samples were tested, as shown in Fig. 12. The mass loss was shown in the TG figure and the peaks referred to different material loss in the DTG figure. Take SSM as an example, the 93% was the residual mass of whole sample and Δ1.6% was the mass loss referring to portlandite. The portlandite change of the EPM was 2.9% while the counterpart of SSM was 1.6%, which demonstrates more portlandite production. A similar foundation was also noticed for calcite when the reduction of the EPM was 1.7% and the reduction of the SSM was 0.76%. The difference of <100°C is difficult to make a contrast because the raw water content was different and the C—S—H decomposition occurred. The summary can be made that the hydration level of EPM was higher. The difference between the SSM and EPM was made by a higher water proportion that promoted the hydration degree. By contrast, the influence of amorphous SiO_2 in the EP was not recognized. The EPCM had the same raw material and mixing proportion with the EPM, except the impregnated PCM. Comparing the residual mass of 86% and 82%, the mass loss of the EPCM was higher than that of the EPM, which referred to the ettringite and partial C—S—H mass. The proportion of ettringite in the EPCM was likely higher but this estimation was not convincing enough. The loss of water content and C—S—H also played a significant role in this temperature range, so more evidence was demanded in the following tests. However, it was related to the hydration process because the mass of PCM accounts for only 1% of the raw material that was negligible. The reductions referring portlandite (2.9% and 2.8%) and calcite (1.7% and 1.9%) of the EPM and EPCM were very close. The peak in the EPCM showed a left shift and the actual value was closer. In summary, the effect of the PCM mainly occurred at the ettringite while the rest of the product showed little change. The SO_4^{2-} in the PCM promotes the production of ettringite.

Isothermal Calorimetry

To reveal the reason for thermal–mechanical changes, the isothermal calorimetry was performed as shown in Fig. 13. The main peak of the SSM was found at 14 h with a start at 5 h. When the aggregate was replaced by the EP, the hydration was prolonged with the peak delayed to 16.2 h and the lower peak value. From the mix strategy, a higher w=c ratio and more SP were used, which were reasons for the hydration peak changing. The accumulated heat of the EPM exceeded its SSM counterpart at 30 h, which was also in accord with a high w=c ratio, meaning a higher level of hydration. In this case, the cement matrix was stronger, but the EP was still weak, which proved the aforementioned deduction.

The peak of the EPCM was hastened to 10 h, which was attributed to the NS attached to the surface of the EPC. The NS was

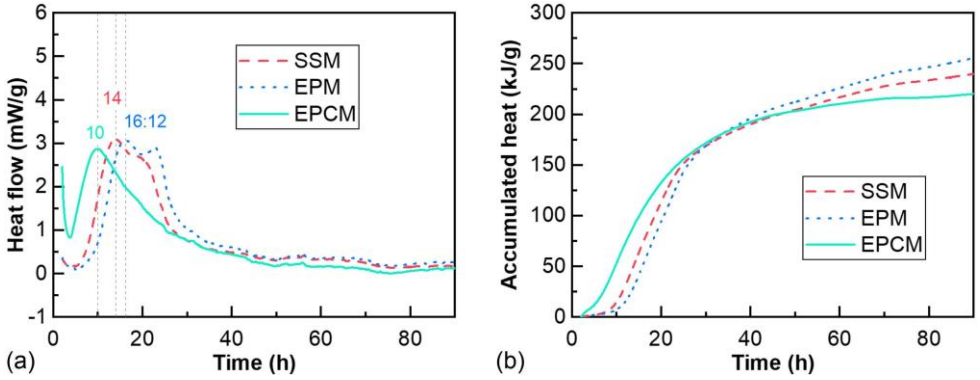

Fig. 13. Isothermal calorimetry for mortars to investigate cement hydration: (a) heat flow for mortar; and (b) heat accumulation for mortar.

universally used to accelerate hydration and boost early strength. However, the accumulated heat was the lowest that contributed to the lowest strength, as already presented. Another noticeable change was the number of main peaks, which was reduced from two to one after the PCM incorporation. The isothermal calorimetry was based on the generated heat from the material. After the first peak, the PCM started work and absorbed the partial heat that covered the second hydration peak (Snehal and Das 2023). In addition, the lower temperature led to a weaker hydration speed that reduced the second peak. As mentioned, the temperature went down from the second day and the PCM released heat, which summarily did not affect the final accumulated heat result.

In this experiment, the NS brought hydration forward but made lower accumulated heat, which was in accord with a traditional effect although cooperated with the NHP. The effect of PCM on cement hydration may be various. Wang et al. (2021) tested the heat flow of mortar incorporation capric acid–based SSPCM. The curves of all samples showed similar regulation and no peak shift was observed, although the increased peak value was found. The different results could be caused by material type, incorporation method, casting method, and so on, which deserved further research. Therefore, the selection of PCM should take the possible hydration reaction into consideration.

SEM-EDS

As shown in Fig. 14, the SSM illustrates the obvious boundary and minor cracks along the aggregate. This could destroy the integrity and form a weak area, which is adverse for mortar strength. Oppositely, the EPM and EPCM show a denser ITZ and nearly no crack occurs around the aggregate. The EP is porous with an extremely high absorption effect due to capillaries. The water absorption (by expanded perlite) and reaction with cement are simultaneous, while inter curing effect is important. The cement paste suction is after the water absorption (Qiu et al. 2023). More importantly, a part of the water is absorbed by the EP, then, leads to an internal curing effect, which is the critical reason for a denser ITZ (Qiu et al. 2023). The weak spot in the SSM is modified, which is the main reason for the strength enhancement. However, the structure of the EP is more brittle than the SS and the enhancement effectiveness will be partly offset. The figures explain the changing strength of the SSM and EPM, except for the EPCM. Chemical elements S (sulfur) and P (phosphorus) were slightly observed on the aggregate of SSM, while they should not be observed from the aggregate. This was caused by the sample preparation, especially the cutting process, which transferred and dispersed the element on the cutting plane. The uneven cross section of the EPM aggregate presented little S and P residual. For EPCM, the concentration rose again and only the deepest part showed black due to the limitation of the scanning ability, which proves the existence of NS and NHP in the aggregate. Then, the microstructure and product at higher magnification are shown in Fig. 15.

All SEM images shown in Fig. 15 were captured around the aggregate. After thorough scanning the area near aggregates, commonly main products, CaðOHÞ$_2$ and C—S—H, were distributed as expected. The SSM showed the lowest compactness and most obvious cracks. That was improved in the EP and EPCM. Based on the universal cement hydration process, ettringite was mainly

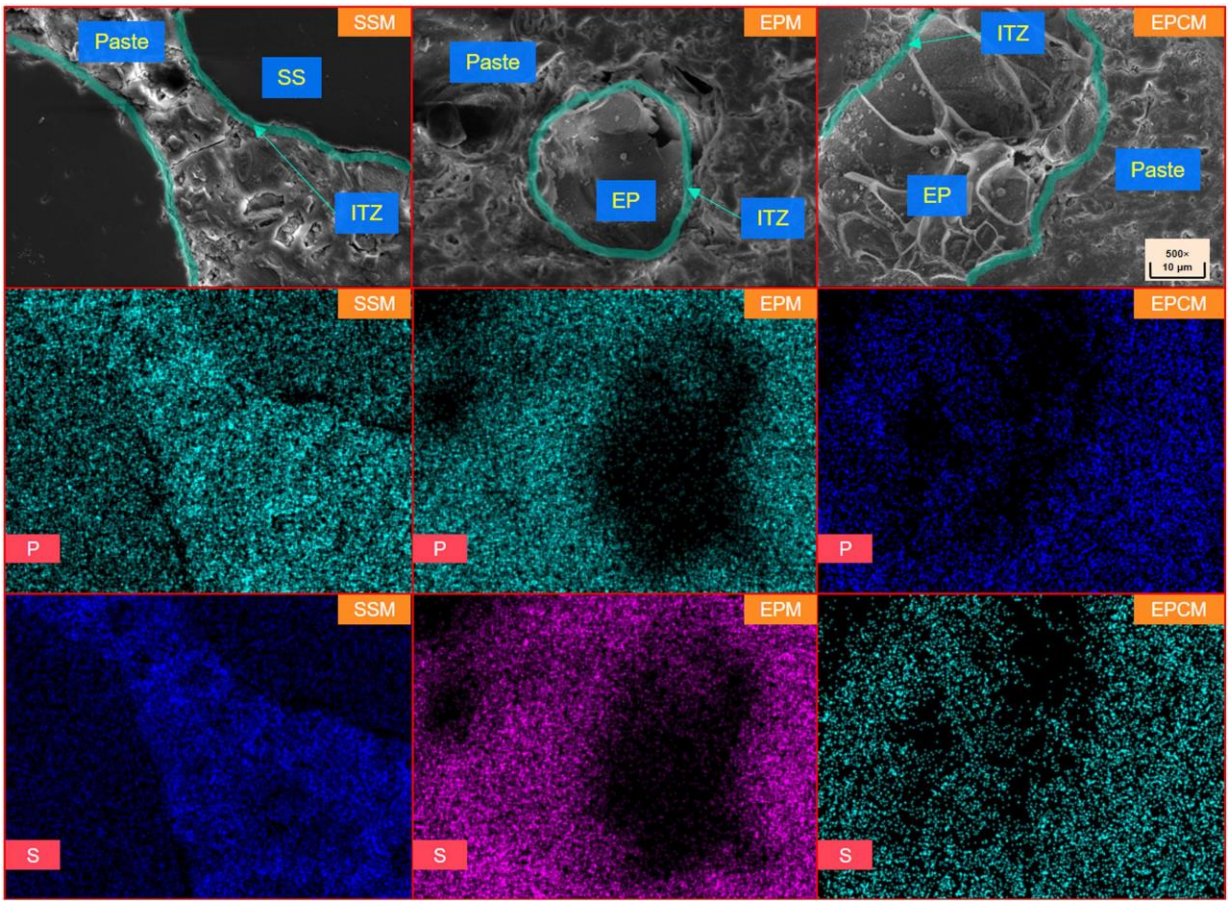

Fig. 14. SEM-EDS result at the magnification of 500×.

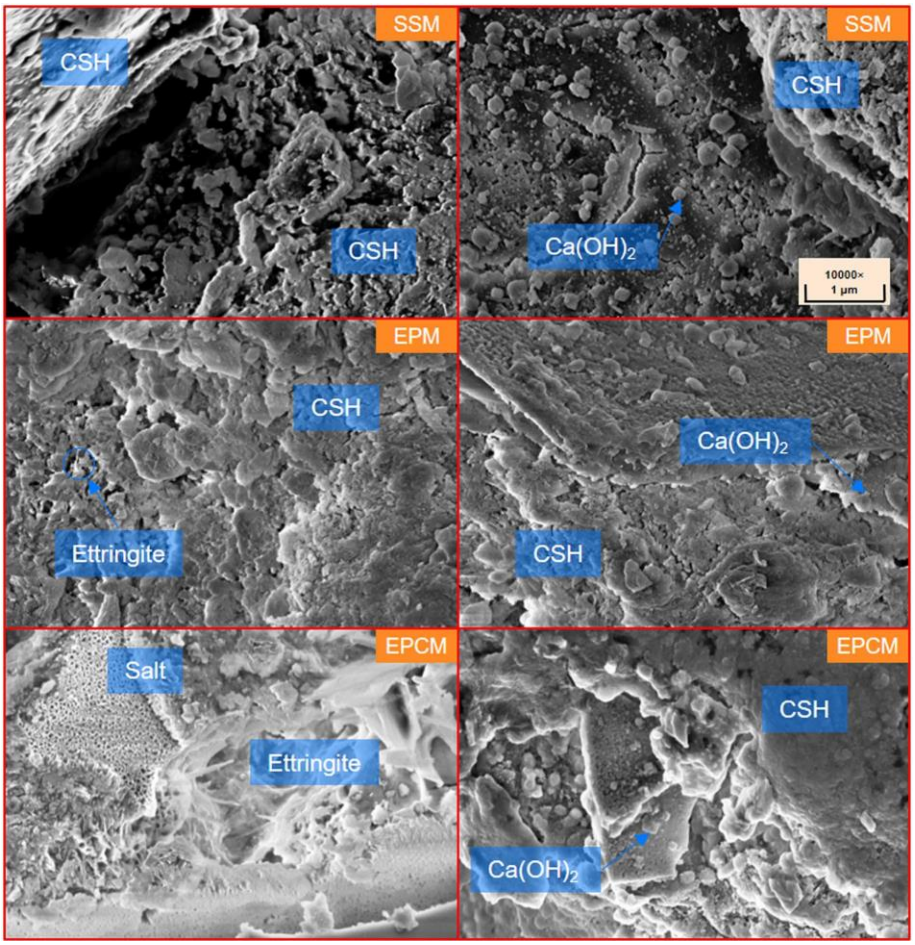

Fig. 15. Microstructure and product at the magnification of 10,000×.

generated in the early stage and was consumed later. These results wwere taken on the 28th day when a large amount of ettringite was consumed. A few minor ettringites were observed in the SSM and EPM, while the EPCM counterpart was relatively significant. In addition, the salt with a compact porous structure was found near the ettringite. It proved the aforementioned analyses that the salt-based inorganic PCM in this experiment boosted the ettringite generation, which was an important reason for the strength reduction.

Conclusions

This study investigated the hydration performance and structure changes of PCM-infused concrete. PCMs are functional additives that have varying influences on cement hydration. Based on the selected material and method in this study, the PCM composite alters hydration performance and temperature evolution. Differences in physical properties are observed, and the significant reasons behind are proposed. The main results are summarized as follows:

1. The impact of the PCM on temperature regulation is remarkable during hydration. The increasing and decreasing temperature trend is kept but the peak is replaced by a plateau. In this experiment, the plateau occurs at roughly 27.8°C. It proves that the PCM works in this period and may influence cement hydration if the phase-changing point is in the specific range.
2. The strength loss is obvious while the compressive strength (reduction of 42%) is more sensitive than the flexural one (reduction of 18%). The testing results primarily attribute this to the bonding quality. A clear gap exists around the aggregate for the reference sample SSM. The porous aggregate benefits the bond quality but the influence of PCM is still critical. The PCM on the surface of the EP changes the hydration product, ettringite, reducing the bond strength.
3. The SSM and EPM presented continuous shrinkage at the early stage, while the EPCM showed expansion reaching the highest value on the 5th day, and the expansion was neutralized until the 8th day. The important part of the PCM, NS, speeds up the cement hydration and boosts the ettringite, which is the main reason for the early stage expansion. The amount of NS is small and the maximum expansion ratio reached 180 $\mu\varepsilon$.
4. The PCM modifies the hydration process based on the isothermal calorimetry results. The thermal peak is reduced although the hydration starts earlier, which is contributed to the NS. The final accumulated heat of the EPCM is the lowest, presenting the lowest hydration level. This result illustrates the quality of the cement matrix that is regarded as another important reason for the reduced mechanical properties of the EPCM. In addition, this analysis is supported by the TGA test results.
5. The pozzolanic reaction of amorphous quartz in the EP is not observed in this experiment. No evidence proves that the difference in hydration product and process is caused by the amorphous quartz. Based on the result of this work, the observed changes between the SSM and EPM are affected by the physical properties such as high water absorption of the EP. The inadequate alkalinity may be the principal reason why it does not trigger the reaction of amorphous quartz.

6. Hydrated salt PCM normally loses most water molecules around 100°C, which transfer to gas. The large gas expansion inside the mortar poses dangerous pressure on the structure. It is suggested that hydrated salt PCM is more suitable for covering the layer instead of bearing stress structure.
7. The chemical property of the PCM influences the hydration adversely, which is supposed to be avoided. It is suggested that the selection of the PCM should match incorporation considering the application environment. The PCM, which may reduce the cement hydration quality, demands higher leakage prevention. It will be better if a PCM is designed that boosts cement hydration. The PCM regulating temperature in the hydration process deserves much attention before application if the used cement type is temperature sensitive.

Data Availability Statement

All data, models, and code generated or used during the study appear in the published paper.

Acknowledgments

The authors appreciate the support from the Australian Research Council (ARC), Australia (FT220100177; LP230100288; DP220100036; DP220101051; IH200100010). Xiaonan Wang and Yipu Guo thank the China Scholarship Council (CSC).

References

Adesina, A. 2019. "Use of phase change materials in concrete: Current challenges." *Renewable Energy Environ. Sustainability* 4 (Aug): 9. https://doi.org/10.1051/rees/2019006.

Akeiber, H., P. Nejat, M. Z. A. Majid, M. A. Wahid, F. Jomehzadeh, I. Zeynali Famileh, J. K. Calautit, B. R. Hughes, and S. A. Zaki. 2016. "A review on phase change material (PCM) for sustainable passive cooling in building envelopes." *Renewable Sustainable Energy Rev.* 60 (Jul): 1470–1497. https://doi.org/10.1016/j.rser.2016.03.036.

Arumugam, C., and S. Shaik. 2021. "Air-conditioning cost saving and CO_2 emission reduction prospective of buildings designed with PCM integrated blocks and roofs." *Sustainable Energy Technol. Assess.* 48 (Dec): 101657. https://doi.org/10.1016/j.seta.2021.101657.

AS (Australian Standard). 2006. *Methods of testing Portland, blended and masonry cements Determination of drying shrinkage of cement mortars*. AS 2350.13-2006. Sydney, NSW, Australia: Standards Australia.

ASTM. 2017. *Standard test method for length change of hardened hydraulic-cement mortar and concrete*. ASTM C157/C157M-17. West Conshohocken, PA: ASTM.

ASTM. 2018. *Standard test method for compressive strength of hydraulic-cement mortars (using portions of prisms broken in flexure)*. ASTM C349-18. West Conshohocken, PA: ASTM.

ASTM. 2021. *Standard test method for flexural strength of hydraulic-cement mortars*. ASTM C348-21. West Conshohocken, PA: ASTM.

AUSPERL. 2021. "Our Company—AUSPERL—Australian Perlite." Accessed July 1, 2021. https://www.ausperl.com.

Brooks, A. L., Y. Fang, Z. Shen, J. Wang, and H. Zhou. 2021. "Enabling high-strength cement-based materials for thermal energy storage via fly-ash cenosphere encapsulated phase change materials." *Cem. Concr. Compos.* 120 (Jul): 104033. https://doi.org/10.1016/j.cemconcomp.2021.104033.

BSI (British Standards Institution). 2002. *Products and systems for the protection and repair of concrete structures—Test methods—Part 4: Determination of shrinkage and expansion*. BS EN 12617-4. London: BSI.

Cao, J., Y. He, J. Feng, S. Lin, Z. Ling, Z. Zhang, and X. Fang. 2020. "Mini-channel cold plate with nano phase change material emulsion for Li-ion battery under high-rate discharge." *Appl. Energy* 279 (Dec): 115808. https://doi.org/10.1016/j.apenergy.2020.115808.

Chen, Y., Y. Huang, S. Wang, and Y. Mu. 2023. "Effects of phase change materials on the freeze–thaw performance of expansive soil." *J. Mater. Civ. Eng.* 35 (7): 04023206. https://doi.org/10.1061/JMCEE7.MTENG-15205.

Cui, H., S. Yu, X. Cao, and H. Yang. 2022a. "Evaluation of printability and thermal properties of 3D printed concrete mixed with phase change materials." *Energies* 15 (6): 1978. https://doi.org/10.3390/en15061978.

Cui, H., J. Zou, Z. Gong, D. Zheng, X. Bao, and X. Chen. 2022b. "Study on the thermal and mechanical properties of steel fibre reinforced PCM-HSB concrete for high performance in energy piles." *Constr. Build. Mater.* 350 (Oct): 128822. https://doi.org/10.1016/j.conbuildmat.2022.128822.

Deb, R., J. He, G. Mishra, and Y. Farnam. 2024a. "Investigating temperature change rate and pore confinement effect on thermal properties of phase change materials for de-icing and low-temperature applications in cementitious composites." *Constr. Build. Mater.* 411 (Jan): 134237. https://doi.org/10.1016/j.conbuildmat.2023.134237.

Deb, R., N. Shrestha, K. Phan, M. Cissao, P. Namakiaraghi, Y. Alqenai, S. Visvalingam, A. Mutua, and Y. A. Farnam. 2024b. "Development of self-heating concrete using low-temperature phase change materials: Multiscale and in situ real-time evaluation of snow-melting and freeze–thaw performance." *J. Mater. Civ. Eng.* 36 (6): 04024102. https://doi.org/10.1061/JMCEE7.MTENG-17048.

Drissi, S., T.-C. Ling, K. H. Mo, and A. Eddhahak. 2019. "A review of microencapsulated and composite phase change materials: Alteration of strength and thermal properties of cement-based materials." *Renewable Sustainable Energy Rev.* 110 (Aug): 467–484. https://doi.org/10.1016/j.rser.2019.04.072.

Elmarghany, M. R., A. Radwan, M. A. Shouman, A. A. Khater, M. S. Salem, and O. Abdelrehim. 2022. "Year-long energy analysis of building brick filled with phase change materials." *J. Energy Storage* 50 (Jun): 104605. https://doi.org/10.1016/j.est.2022.104605.

Esmaeeli, H. S., Y. Farnam, J. E. Haddock, P. D. Zavattieri, and W. J. Weiss. 2018. "Numerical analysis of the freeze-thaw performance of cementitious composites that contain phase change material (PCM)." *Mater. Des.* 145 (May): 74–87. https://doi.org/10.1016/j.matdes.2018.02.056.

Fang, Y., M. R. Ahmad, J.-C. Lao, L.-P. Qian, and J.-G. Dai. 2023. "Development of artificial geopolymer aggregates with thermal energy storage capacity." *Cem. Concr. Compos.* 135 (Jan): 104834. https://doi.org/10.1016/j.cemconcomp.2022.104834.

Farnam, Y., M. Krafcik, L. Liston, T. Washington, K. Erk, B. Tao, and J. Weiss. 2016. "Evaluating the use of phase change materials in concrete pavement to melt ice and snow." *J. Mater. Civ. Eng.* 28 (4): 04015161. https://doi.org/10.1061/(ASCE)MT.1943-5533.0001439.

Farnam, Y., A. Wiese, D. Bentz, J. Davis, and J. Weiss. 2015. "Damage development in cementitious materials exposed to magnesium chloride deicing salt." *Constr. Build. Mater.* 93 (Sep): 384–392. https://doi.org/10.1016/j.conbuildmat.2015.06.004.

Haider, M. Z., X. Jin, R. Sharma, J. Pei, and J. W. Hu. 2022. "Enhancing the compressive strength of thermal energy storage concrete containing a low-temperature phase change material using silica fume and multi-walled carbon nanotubes." *Constr. Build. Mater.* 314 (Jan): 125659. https://doi.org/10.1016/j.conbuildmat.2021.125659.

Hirschey, J., M. Goswami, D. O. Akamo, N. Kumar, Y. Li, T. J. LaClair, K. R. Gluesenkamp, and S. Graham. 2022. "Effect of expanded graphite on the thermal conductivity of sodium sulfate decahydrate ($Na_2SO_4 \cdot 10H_2O$) phase change composites." *J. Energy Storage* 52 (Aug): 104949. https://doi.org/10.1016/j.est.2022.104949.

Hosseinzadeh, K., E. Montazer, M. B. Shafii, and A. R. D. Ganji. 2021. "Solidification enhancement in triplex thermal energy storage system via triplets fins configuration and hybrid nanoparticles." *J. Energy Storage* 34 (Feb): 102177. https://doi.org/10.1016/j.est.2020.102177.

Hou, J., Z.-A. Liu, L. Zhang, T. Zhang, C. Hou, and H. Fukuda. 2023. "Parametric and economic analysis of incorporating phase change material (PCM) into exterior walls to reduce energy demand for traditional dwellings in northeast of Sichuan hills, China." *Appl. Therm.*

Eng. 223 (Mar): 119982. https://doi.org/10.1016/j.applthermaleng.2023.119982.

Hu, Y., P. Kvols Heiselberg, C. Drivsholm, A. Skød Søvsø, P. J. C. Vogler-Finck, and K. Kronby. 2021. "Experimental and numerical study of PCM storage integrated with HVAC system for energy flexibility." *Energy Build.* 255 (Jan): 111651. https://doi.org/10.1016/j.enbuild.2021.111651.

Hunger, M., A. G. Entrop, I. Mandilaras, H. J. H. Brouwers, and M. Founti. 2009. "The behavior of self-compacting concrete containing micro-encapsulated phase change materials." *Cem. Concr. Compos.* 31 (10): 731–743. https://doi.org/10.1016/j.cemconcomp.2009.08.002.

Islam, M. N., and D. H. Ahmed. 2021. "Delaying the temperature fluctuations through PCM integrated building walls—Room conditions, PCM placement, and temperature of the heat sources." *Energy Storage* 3 (5): e245. https://doi.org/10.1002/est2.245.

Kumar, D., M. Alam, and J. Sanjayan. 2022. "An energy-efficient form-stable phase change materials synthesis method to enhance thermal storage and prevent acidification of cementitious composite." *Constr. Build. Mater.* 348 (Sep): 128697. https://doi.org/10.1016/j.conbuildmat.2022.128697.

Kuznik, F., D. David, K. Johannes, and J.-J. Roux. 2011. "A review on phase change materials integrated in building walls." *Renewable Sustainable Energy Rev.* 15 (1): 379–391. https://doi.org/10.1016/j.rser.2010.08.019.

Li, D., R. Yang, M. Arıcı, B. Wang, E. Tunçbilek, Y. Wu, C. Liu, Z. Ma, and Y. Ma. 2022. "Incorporating phase change materials into glazing units for building applications: Current progress and challenges." *Appl. Therm. Eng.* 210 (Jun): 118374. https://doi.org/10.1016/j.applthermaleng.2022.118374.

Li, W., C. Ling, Z. Jiang, and Q.-Q. Yu. 2019. "Evaluation of the potential use of form-stable phase change materials to improve the freeze-thaw resistance of concrete." *Constr. Build. Mater.* 203 (Apr): 621–632. https://doi.org/10.1016/j.conbuildmat.2019.01.098.

Mi, X., R. Liu, H. Cui, S. A. Memon, F. Xing, and Y. Lo. 2016. "Energy and economic analysis of building integrated with PCM in different cities of China." *Appl. Energy* 175 (Aug): 324–336. https://doi.org/10.1016/j.apenergy.2016.05.032.

Nayak, S., N. M. A. Krishnan, and S. Das. 2019. "Microstructure-guided numerical simulation to evaluate the influence of phase change materials (PCMs) on the freeze-thaw response of concrete pavements." *Constr. Build. Mater.* 201 (Mar): 246–256. https://doi.org/10.1016/j.conbuildmat.2018.12.199.

Pilehvar, S., V. D. Cao, A. M. Szczotok, L. Valentini, D. Salvioni, M. Magistri, R. Pamies, and A.-L. Kjøniksen. 2017. "Mechanical properties and microscale changes of geopolymer concrete and Portland cement concrete containing micro-encapsulated phase change materials." *Cem. Concr. Res.* 100 (Oct): 341–349. https://doi.org/10.1016/j.cemconres.2017.07.012.

Pilehvar, S., A. M. Szczotok, J. F. Rodríguez, L. Valentini, M. Lanzón, R. Pamies, and A.-L. Kjøniksen. 2019. "Effect of freeze-thaw cycles on the mechanical behavior of geopolymer concrete and Portland cement concrete containing micro-encapsulated phase change materials." *Constr. Build. Mater.* 200 (Mar): 94–103. https://doi.org/10.1016/j.conbuildmat.2018.12.057.

Qiu, X., W. Chen, L. Li, H. Li, and H. Liu. 2023. "The effects of particle sizes of expanded perlite on the mechanical properties and chloride penetration resistance of ECCs." *J. Build. Eng.* 78 (Nov): 107706. https://doi.org/10.1016/j.jobe.2023.107706.

Ramakrishnan, S., J. Sanjayan, X. Wang, M. Alam, and J. Wilson. 2015. "A novel paraffin/expanded perlite composite phase change material for prevention of PCM leakage in cementitious composites." *Appl. Energy* 157 (Nov): 85–94. https://doi.org/10.1016/j.apenergy.2015.08.019.

Ramakrishnan, S., X. Wang, J. Sanjayan, E. Petinakis, and J. Wilson. 2017. "Development of thermal energy storage cementitious composites (TESC) containing a novel paraffin/hydrophobic expanded perlite composite phase change material." *Sol. Energy* 158 (Dec): 626–635. https://doi.org/10.1016/j.solener.2017.09.064.

Rao, Z., T. Xu, C. Liu, Z. Zheng, L. Liang, and K. Hong. 2018. "Experimental study on thermal properties and thermal performance of eutectic hydrated salts/expanded perlite form-stable phase change materials for passive solar energy utilization." *Sol. Energy Mater. Sol. Cells* 188 (Dec): 6–17. https://doi.org/10.1016/j.solmat.2018.08.012.

Rathore, P. K. S., and S. K. Shukla. 2020. "An experimental evaluation of thermal behavior of the building envelope using macroencapsulated PCM for energy savings." *Renewable Energy* 149 (Apr): 1300–1313. https://doi.org/10.1016/j.renene.2019.10.130.

Ravasio, L., R. K. Calay, and R. Riise. 2021. "Simplified thermal performance evaluation of a PCM-filled triple-glazed window under arctic climate conditions." *Energies* 14 (23): 8068. https://doi.org/10.3390/en14238068.

Ren, M., X. Wen, X. Gao, and Y. Liu. 2021. "Thermal and mechanical properties of ultra-high performance concrete incorporated with micro-encapsulated phase change material." *Constr. Build. Mater.* 273 (Mar): 121714. https://doi.org/10.1016/j.conbuildmat.2020.121714.

Šavija, B. 2018. "Smart crack control in concrete through use of phase change materials (PCMs): A review." *Materials* 11 (5): 654. https://doi.org/10.3390/ma11050654.

Šavija, B., and E. Schlangen. 2016. "Use of phase change materials (PCMs) to mitigate early age thermal cracking in concrete: Theoretical considerations." *Constr. Build. Mater.* 126 (Nov): 332–344. https://doi.org/10.1016/j.conbuildmat.2016.09.046.

Snehal, K., and B. B. Das. 2023. "Effect of phase-change materials on the hydration and mineralogy of cement mortar." *Proc. Inst. Civ. Eng. Constr. Mater.* 176 (3): 117–127. https://doi.org/10.1680/jcoma.20.00045.

Snehal, K., B. B. Das, and S. Barbhuiya. 2022. "Influence of aggressive exposure on the degradation of nano-silica admixed cementitious mortar integrated with phase change materials." *Constr. Build. Mater.* 335 (Jun): 127467. https://doi.org/10.1016/j.conbuildmat.2022.127467.

Snehal, K., B. B. Das, and S. Kumar. 2020. "Influence of integration of phase change materials on hydration and microstructure properties of nanosilica admixed cementitious mortar." *J. Mater. Civ. Eng.* 32 (6): 04020108. https://doi.org/10.1061/(ASCE)MT.1943-5533.0003178.

Snoeck, D., B. Priem, P. Dubruel, and N. De Belie. 2016. "Encapsulated phase-change materials as additives in cementitious materials to promote thermal comfort in concrete constructions." *Mater. Struct.* 49 (1): 225–239. https://doi.org/10.1617/s11527-014-0490-5.

Song, C., Y. C. Choi, and S. Choi. 2016. "Effect of internal curing by superabsorbent polymers—Internal relative humidity and autogenous shrinkage of alkali-activated slag mortars." *Constr. Build. Mater.* 123 (Oct): 198–206. https://doi.org/10.1016/j.conbuildmat.2016.07.007.

Sun, J., J. Zhao, W. Zhang, J. Xu, B. Wang, X. Wang, J. Zhou, H. Guo, and Y. Liu. 2023. "Composites with a novel core–shell structural expanded perlite/polyethylene glycol composite PCM as novel green energy storage composites for building energy conservation." *Appl. Energy* 330 (Jan): 120363. https://doi.org/10.1016/j.apenergy.2022.120363.

Urgessa, G., K.-K. Yun, J. Yeon, and J. H. Yeon. 2019. "Thermal responses of concrete slabs containing microencapsulated low-transition temperature phase change materials exposed to realistic climate conditions." *Cem. Concr. Compos.* 104 (Nov): 103391. https://doi.org/10.1016/j.cemconcomp.2019.103391.

Wang, X., W. Li, Y. Huang, S. Zhang, and K. Wang. 2023. "Study on shape-stabilised paraffin-ceramsite composites with stable strength as phase change material (PCM) for energy storage." *Constr. Build. Mater.* 388 (Jul): 131678. https://doi.org/10.1016/j.conbuildmat.2023.131678.

Wang, X., W. Li, Z. Luo, K. Wang, and S. P. Shah. 2022. "A critical review on phase change materials (PCM) for sustainable and energy efficient building: Design, characteristic, performance and application." *Energy Build.* 260 (Apr): 111923. https://doi.org/10.1016/j.enbuild.2022.111923.

Wang, Y., J. Li, W. Miao, Y. Su, X. He, and B. Strnadel. 2021. "Preparation and characterizations of hydroxyapatite microcapsule phase change materials for potential building materials." *Constr. Build. Mater.* 297 (Aug): 123576. https://doi.org/10.1016/j.conbuildmat.2021.123576.

Xie, S., C. Ma, Z. Ji, Z. Wu, T. Si, Y. Wang, and J. Wang. 2023. "Electromagnetic wave absorption and heat storage dual-functional cement composites incorporated with carbon nanotubes and phase change microcapsule." *J. Build. Eng.* 67 (May): 105925. https://doi.org/10.1016/j.jobe.2023.105925.

Xu, B., and Z. Li. 2014. "Performance of novel thermal energy storage engineered cementitious composites incorporating a paraffin/diatomite composite phase change material." *Appl. Energy* 121 (May): 114–122. https://doi.org/10.1016/j.apenergy.2014.02.007.

Xue, C., W. Li, J. Li, and K. Wang. 2019. "Numerical investigation on interface crack initiation and propagation behaviour of self-healing cementitious materials." *Cem. Concr. Res.* 122 (Aug): 1–16. https://doi.org/10.1016/j.cemconres.2019.04.012.

Yu, K., Y. Liu, M. Jia, C. Wang, and Y. Yang. 2022. "Thermal energy storage cement mortar containing encapsulated hydrated salt/fly ash cenosphere phase change material: Thermo-mechanical properties and energy saving analysis." *J. Energy Storage* 51 (Jul): 104388. https://doi.org/10.1016/j.est.2022.104388.

Zhang, G., N. Xiao, B. Wang, and A. G. Razaqpur. 2022. "Thermal performance of a novel building wall incorporating a dynamic phase change material layer for efficient utilization of passive solar energy." *Constr. Build. Mater.* 317 (Jan): 126017. https://doi.org/10.1016/j.conbuildmat.2021.126017.

Zhang, X., R. Wen, C. Tang, B. Wu, Z. Huang, X. Min, Y. Huang, Y. Liu, M. Fang, and X. Wu. 2016. "Thermal conductivity enhancement of polyethylene glycol/expanded perlite with carbon layer for heat storage application." *Energy Build.* 130 (Oct): 113–121. https://doi.org/10.1016/j.enbuild.2016.08.049.

Zhang, Y., Z. Zhang, J. Zhou, and Y. Wang. 2020. "Mechanical and thermal properties of phase change energy storage concrete." *J. Phys.: Conf. Ser.* 1549 (3): 032110. https://doi.org/10.1088/1742-6596/1549/3/032110.